PROCEEDINGS OF SCIENCE

Modeling of Gamma Ray Burst (GRB) Afterglow at Very High Energy (VHE) regime

Tanima Mondal,[a,*] **Lekshmi Resmi**[b] **and Debanjan Bose**[c]

[a] *Department of Physics, Indian Institute of Technology Kharagpur*
Kharagpur, West Bengal 721302, India

[b] *Department of Earth & Space Sciences, Indian Institute of Space Science & Technology*
Trivandrum 695547, India

[c] *School of Astrophysics, Presidency University*
Kolkata, West Bengal 700073, India

E-mail: mtanima14@gmail.com, l.resmi@gmail.com, debaice@gmail.com

MAGIC and HESS's detection of delayed VHE gamma-rays from Gamma-Ray Bursts (GRBs) has demonstrated the promising future of GRB afterglow studies with the Cherenkov Telescope Array (CTA). We have developed a model where we have explored the afterglow parameter space to see the detectability of sub-TeV photons by CTA. The spectral energy distribution is computed using a one-zone electron synchrotron and a synchrotron self-Compton model at a given redshift. We find that jets with high kinetic energy decelerating into a dense ambient medium are better candidates for CTA. In this paper, we have applied our model to fit the spectrum of a long GRB detected by MAGIC. The result indicates that our model can well fit EBL attenuated MAGIC afterglow spectrum.

38th International Cosmic Ray Conference (ICRC2023)
26 July - 3 August 2023
Nagoya, Japan

ICRC2023
38th International Cosmic Ray Conference
The Astroparticle Physics Conference

*Speaker

© Copyright owned by the author(s) under the terms of the Creative Commons Attribution-NonCommercial-NoDerivatives 4.0 International License (CC BY-NC-ND 4.0).

PoS(ICRC2023)600

1. Introduction

Gamma-ray bursts(GRB) are the most intense and luminous electromagnetic explosions through the abrupt emission of gamma-ray photons. They are catastrophic stellar events, last for a few milliseconds to thousands of seconds, and release huge amounts of isotropic Energy $\sim 10^{49} - 10^{53}$ erg[1]. They are isotropically distributed in the sky, which indicates their extra-galactic origin[2]. They provide the best opportunities for multimessenger observations of non-electromagnetic signals, which include cosmic rays, gravitational waves, and very high energy (VHE) neutrinos. Based on the observed duration of Gamma-ray bursts, they are categorized into two distinct types: Long GRB (LGRB, last more than 2 sec) and Short GRB (SGRB, last for less than 2 sec)[3]. GRB Fireball model depicts that the radiation coming out from the compact object in the form of a relativistic jet has an initial prompt emission phase and, subsequently, an afterglow phase. The prompt emission phase occurs through the dissipation of kinetic energy of the internal shocks within the jet. This phase emits highly variable radiation of energy in a few keV-MeV bands[3], which lasts for milliseconds to a few minutes. The afterglow phase results due to the interaction between the circumburst medium and relativistic outflow and can last for a longer time window. The slowly fading radiation emitted in this phase expands throughout the electromagnetic spectrum, from low-frequency radio to very high-frequency (GeV-TeV)[4] gamma-ray band.

The detection of GRB afterglow phase is very significant, as it constrains many physical parameters of GRB jets and of the surrounding medium. They reveal fundamental information on particle acceleration mechanisms, radiation mechanisms, and the progenitor of GRBs. Recently sub-TeV photons have been detected by HESS[5] and MAGIC[6] telescopes from a couple of GRBs. These sub-TeV photons detected in the afterglow phase of GRBs are attributed to the high burst energies and low redshifts. Presently, we have developed a model on GRB afterglow emission, particularly on the very high energy(VHE) gamma-ray band. This afterglow emission can be well explained by one-zone electron synchrotron and synchrotron self-Compton(SSC) model[7–9]. Our model can estimate the intrinsic flux of those VHE GRB afterglows and can predict the detectable flux for ground-based detectors after correcting it for EBL absorption. Through our model, Cherenkov Telescope Array(CTA), the next-generation gamma-ray observatory, can predict whether GRB afterglows will be detected at this VHE domain or not.

Based on our afterglow model, here we have predominantly discussed one of those GRBs — GRB 190114C, which MAGIC detected for the first time, reported on 14th January 2019[6]. This GRB was detected at a redshift of z=0.4245. During the first 20 minutes of the observation, the sub-TeV photons reached the energy range of $0.2 \leq E \leq 1$ TeV[6].

This paper is organized as follows. In section-2, we have briefly summarised the model we developed to explain GRB afterglow emission in the VHE regime. In section-3, we have invoked our model on MAGIC detected long GRB 190114C to fit the afterglow MAGIC spectrum. Finally, in section-4, we have summarized the paper.

2. Overview of our afterglow model for Very High Energy (VHE) regime

The Cherenkov Telescope Array (CTA), the next-generation gamma-ray observatory, will be able to conduct studies of GRB afterglow owing to the detection of delayed sub-TeV photons from

PoS(ICRC2023)600

GRBs by MAGIC and HESS. Afterglow detection rates are anticipated to rise sharply due to the CTA's exceptional sensitivity. The model [10] we developed allows us to investigate the afterglow parameter space and to predict sub-TeV photon's detectability by CTA. Our model depends on how the ultra-relativistic ejecta and the constant density ISM medium around the burster interact. Both the relativistic ejecta and the ISM medium are considered to have negligible pressure and temperature. The blast wave deceleration is assumed to be adiabatic to ensure that radiative losses from shock downstream are negligible. The parameters that describe the shock afterglow microphysics are — E the isotropic equivalent kinetic energy of the explosion, n_0 the density of the ambient medium, Γ_0 the initial bulk Lorentz factor of the relativistic outflow, p the power-law index of the electron energy distribution, ϵ_e the fraction of thermal energy carried by non-thermal electrons, and ϵ_B the fraction of thermal energy transferred to the magnetic field within the emitting region. We have solved three simultaneous ordinary differential equations [10] which describe the evolution of the bulk Lorentz factor of the blast wave, i.e., $\Gamma(r)$ as a function of the observer's time t, in accordance with our work. Our calculations revealed that the numerical and analytical approximation of $\Gamma(r)$ significantly differs at the epoch of deceleration when the peak of the VHE light curve occurs.

The afterglow spectrum of GRB is governed by the broken power-law distribution, where the injected electron distribution $N(\gamma)$ is proportional to γ^{-p}, where γ is the Lorentz factor of the electron. The afterglow spectrum comprises two peaks in spectral energy distribution (SED), where the first peak is governed by synchrotron emission of electrons inside the jet. The second peak is governed by the synchrotron self-Compton emission[11] where the relativistic electrons upscatter synchrotron photons to high energy. This broadband spectrum is multi-segmented and is separated by three distinctive break frequencies —

i. ν_m is the minimum injection frequency at which electrons are accelerated with their minimum Lorentz factor $\gamma_m \propto \epsilon_e \Gamma$, where Γ is the bulk Lorentz factor of the ejected burst.

ii. ν_c^s is the cooling frequency defined by the cooling Lorentz factor $\gamma_c^s \propto \left(n_0\, \epsilon_B\, \Gamma^2\, t\right)^{-1}$, where t is the cooling time scale where electrons lose half of its initial kinetic energy.

iii. ν_{max} is the maximum synchrotron frequency which is defined by maximum synchrotron energy $\gamma_{max} \propto \left(e_{acc}^{1/2}\, n_0^{-1/4} \epsilon_B^{-1/4}\, \Gamma^{-1/2}\right)$ above which electrons can not accelerate efficiently. γ_{max} is determined by comparing the electron's acceleration time-scale and cooling time scale[12, 13]. The factor e_{acc} depicts the efficiency of the acceleration process.

In our calculation, we have considered $e_{acc} = 0.35$, and p=2.2. We have calculated the total synchrotron flux($F_{\nu,syn}$) based on [11, 14] whether a small fraction of electrons has cooled down (slow cooling, $\gamma_m < \gamma_c$) or all the electrons in the distribution have cooled down (fast cooling, $\gamma_m > \gamma_c$).

We have improved our GRB afterglow modeling by invoking the SSC effect on GRB spectrum, as it can explain the origin of sub-TeV photon. In order to accomplish the radiated SSC power (P_{SSC}) from our model, we have described this SSC effect through the Compton Y parameter. Y parameter can be defined as SSC to Synchrotron power ratio i.e. $Y = P_{SSC}/P_{syn}$. Here we have calculated the Y parameter considering the Thomson regime[15]. Being an elastic scattering

PoS(ICRC2023)600

process, the interaction cross-section of Thomson scattering is insensitive to electron or photon energy. Moreover, in the Thomson regime, both P_{SSC} and P_{syn} are proportional to γ^2, which also makes the Y parameter independent of energy. Here Y parameter primarily depends upon two shock microphysical parameters (ϵ_e, ϵ_B) and time t. Hence Y_T becomes $Y_T = Y(\epsilon_e, \epsilon_B, t)$. In this work, we did not consider the KN effect[16] to compute the Y parameter, which significantly reduces scattering cross-section while interacting with the GeV-TeV photon. To obtain the SSC spectrum, we also did not consider optical depth to pair production. We ignored synchrotron self-absorption frequency in our model, as we are modeling the afterglow emission at only the VHE photon bands. In the presence of the Y parameter, SSC power loss is enhanced, and it exceeds that of synchrotron power[12]. Hence in the presence of the SSC cooling effect, the cooling Lorentz factor and cooling frequency can be rewritten as,

$$\begin{aligned} \gamma_c &= \gamma_c^s/(1+Y) \\ \nu_c &= \nu_c^s/(1+Y)^2 \end{aligned} \tag{1}$$

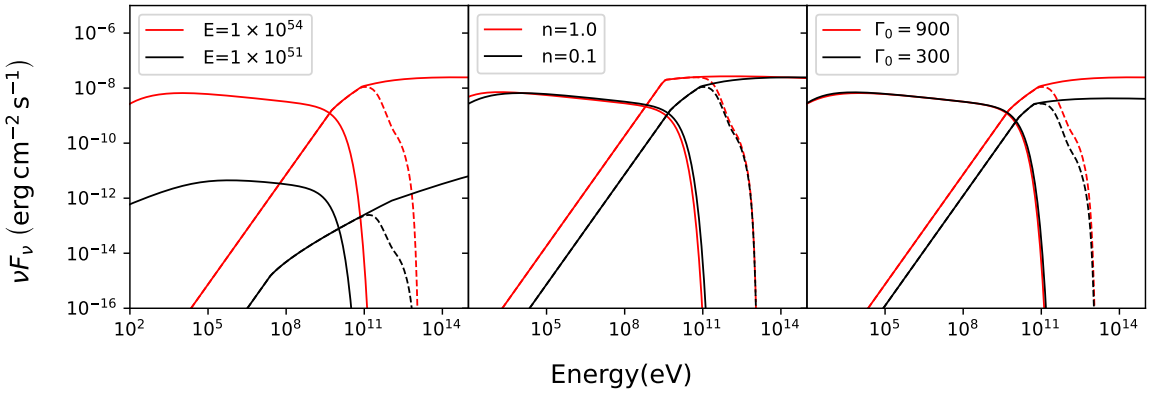

Figure 1: Figure shows the SEDs for different combinations of parameters (E, n_0, and Γ_0) at a given redshift z=0.3. The first panel depicts the spectrum with a variation of E, at fixed $n_0 = 0.1\ cm^{-3}$, $\epsilon_B = 10^{-4}$, ϵ_e= 0.15, $\Gamma_0 = 900$. Subsequently, the second panel represents the spectrum with a variation of n_0, at fixed $E = 1 \times 10^{54}\ erg$, $\epsilon_B = 10^{-4}$, ϵ_e= 0.15, $\Gamma_0 = 900$. The third panel shows the spectrum with a variation of Γ_0, at a fixed $E = 1 \times 10^{54}\ erg$, $\epsilon_B = 10^{-4}$, ϵ_e= 0.15, and $n_0 = 0.1\ cm^{-3}$. For all of the panels, the red solid line represents synchrotron and SSC spectra at higher values of afterglow parameter space. The black solid line represents the synchrotron and SSC spectra at lower values of those parameters. The red and black dashed lines represent the SSC spectra after correcting them for EBL attenuation for higher and lower values of those parameters, respectively.

The VHE part of the GRB afterglow spectrum is significantly affected when VHE gamma photons interact with Extragalactic Background Light (EBL) through pair production [17, 18]. Hence, for any ground-based atmospheric Cherenkov telescopes, the relation between observed flux and intrinsic flux from the source can be written as, $\left(\frac{dF}{dE}\right)_{\rm obs} = \left(\frac{dF}{dE}\right)_{\rm int} \times e^{-\alpha\tau(E,z)}$. Here $\tau(E,z)$ depicts the optical depth of the EBL attenuation factor. In our analysis, we have calculated EBL attenuation factor using EBL Dominguez Model[19] employing the publicly available JetSeT [20] package.

The model we have developed can explain time-evolving SEDs associating both synchrotron and Synchrotron Self Compton (SSC) radiation. It is crucial to conduct an analysis of the GRB

PoS(ICRC2023)600

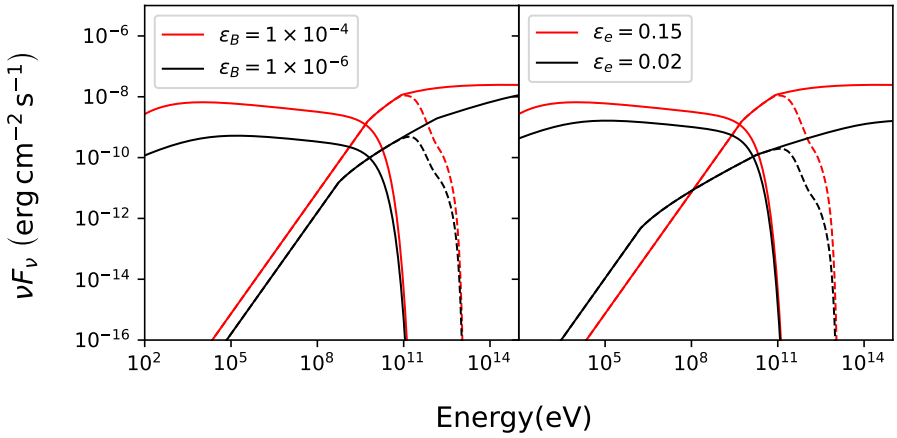

Figure 2: Figure shows the SEDs for different combinations of ϵ_e and ϵ_B for redshift z=0.3. First panel depicts the spectrum with a variation of ϵ_B, at a fixed $E = 1 \times 10^{54}\ erg$, $n_0 = 0.1\ cm^{-3}$, $\Gamma_0 = 900$, ϵ_e=0.15. Second panel represents the spectrum with a variation of ϵ_e, at fixed $E = 1 \times 10^{54}\ erg$, $n_0 = 0.1\ cm^{-3}$, $\Gamma_0 = 900$, and $\epsilon_B = 10^{-4}$.

afterglow parameter space to obtain their detectability in the GeV-TeV regime. Here in our analysis, we consider the redshift z=0.3, and modulate different microphysical parameters in a fixed range. In each instance of our discussion, the electrons are in the slow cooling regime. From the three panels of Figure-1, higher values of E, n_0, and Γ_0 lead to higher values of SSC flux. These three panels have been generated keeping $\epsilon_e = 0.15$, and $\epsilon_B = 1 \times 10^{-4}$ fixed. The dependency of afterglow SSC flux on different parameters can be explained from the analytical expression, $f_\nu^{\rm SSC} \propto E^{4/3} n_0^{1.467} \Gamma_0^{2.933} \epsilon_B^{0.8} \epsilon_e^{2.4}$ [10]. From Figure-2, ee can see how SSC flux is increasing with higher values of ϵ_B and ϵ_e. Here we found that afterglow flux starts dominated by SSC $\sim$ 1 GeV and also got attenuated by EBL at $\sim$ 1 TeV.

3. Application of our VHE afterglow model on Long GRB 190114C

We have fit the spectrum of long GRB 190114C detected by MAGIC employing our model[6]. For this LGRB (isotropic energy $\sim E > 10^{50}$ erg), we showed an EBL-corrected afterglow spectrum and demonstrated how observed broadband spectra can be explained using synchrotron and SSC emission of the afterglow shock wave. Here, we have chosen the best parameter sets based on our model assumptions to fit MAGIC spectrum. We have explored the characteristics of time-evolving spectral energy distribution(SED) and have studied the favourable parameter space. Based on this we can predict the detectability of VHE afterglow emission in the sub-TeV domain.

In this section, we generated SEDs based on our model assumptions discussed in the previous section. SED is computed at an early time epoch of 90 sec (interval: 68-110 sec), and both LAT and MAGIC data points are fitted with our choice of microphysical parameter sets shown in Table-1 below.

The SED spectrum is shown in Figure-3. We found that at the deceleration time t_{dec}, electrons are in the slow cooling regime at $E = 4 \times 10^{54}\ erg$, $n_0 = 0.1\ cm^{-3}$, $\Gamma_0 = 900$. Due to the hydrodynamic evolution of relativistic blast wave, minimum injection frequency ν_m is lower than

PoS(ICRC2023)600

Time (t in sec)	E (in erg)	n_0 (in cm^{-3})	Γ_0	ϵ_e	ϵ_B	Γ	B (in Gauss)	p
90	4×10^{54}	0.1	900	0.15	2×10^{-5}	168.6	0.29	2.2

Table 1: Best-fit parameters obtained from our model for GRB 190114C

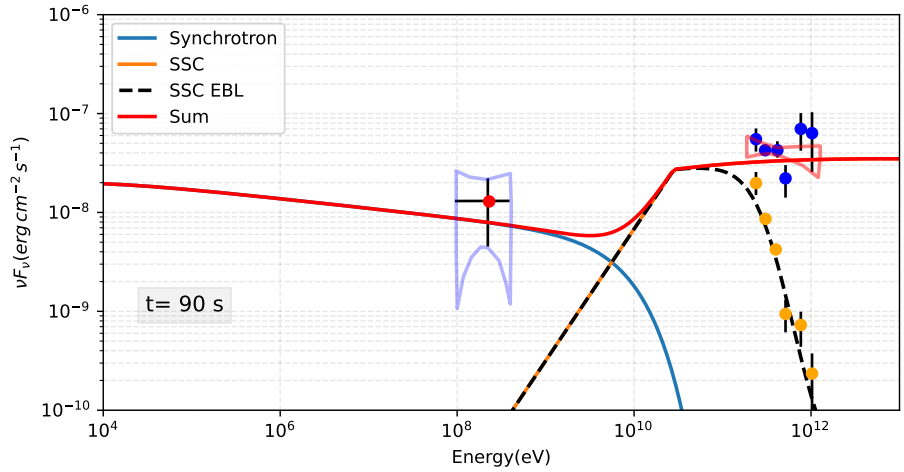

Figure 3: Figure shows synchrotron and SSC spectra of GRB 190114C in a homogeneous ISM medium at redshift z=0.4245, derived from the best-fit parameters mentioned in Table-1. The red circles represent Fermi-LAT data points, the orange circles represent the data detected by MAGIC after correcting for EBL attenuation, and the blue circles represent the same MAGIC data at the source position. The vertical error bars associated with MAGIC EBL corrected data points represent 1σ errors in SSC flux. The contour regions associated with the LAT (red) and MAGIC (blue) data points represent an energy boundary where photons are detected with 1σ error.

cooling frequency ν_c at the early epoch of 90 sec. Along with in Synchrotron-self-Compton(SSC) emission, the break frequency ν_{mm}^{IC} is also lower than ν_{cc}^{IC}. This leads both the synchrotron and SSC emission to be in the slow cooling regime. At this early epoch, synchrotron and SSC peak flux are $1.976 \times 10^{-8}\ erg\ cm^{-2}\ s^{-1}$, and $3.493 \times 10^{-8}\ erg\ cm^{-2}\ s^{-1}$ respectively. Thus, we observed that the synchrotron and SSC flux in the ISM medium of constant density decreased over time in accordance with the broken-power law distribution of non-thermal electrons. In Figure-3, contour regions are also associated with the uncertainty in observed data by MAGIC through vertical and horizontal error bars, corresponding to 1σ error in flux and observed frequency, respectively.

We also have encountered that a higher ϵ_e with higher ϵ_B leads to a higher SSC flux, but keeping the ϵ_e same and reducing ϵ_B decreases the peak SSC flux in the SED. Since lowering the value of ϵ_B, reduces the strength of the magnetic field in the synchrotron self-Compton (SSC) process, hence the peak flux is expected to decrease, and the overall shape of the SED also be affected. Besides, lower values of both ϵ_e and ϵ_B lead to lower values of SSC flux.

4. Conclusion

In this study, we have briefly discussed our VHE afterglow model for redshift z=0.3, showcasing SEDs for different combinations of microphysical parameters. The SSC spectrums in SEDs are

PoS(ICRC2023)600

EBL corrected employing the EBL Dominguez factor. The results describe that higher values of E, n_0, Γ_0 lead to higher SSC flux, which showcase similar characteristics discussed in our model[10]. We also found that higher value of ϵ_e with higher ϵ_B leads to a higher SSC flux.

To show the robustness of our model, we have invoked our analysis on long GRB 190114C and have explored the characteristics of synchrotron and SSC spectrums with a favourable set of parameter space. We found that the Spectral Energy Distribution (SED) curve of GRB 190114C at an early time epoch of 90 sec well fit the MAGIC and LAT data with our choice of model parameters. For redshift z=0.4245, we have calculated EBL corrected SSC flux, which is also well-fitted with the EBL data points of MAGIC.

Acknowledgements

Tanima Mondal acknowledges the support of the Prime Minister's Research Fellowship (PMRF). Tanima Mondal like to thank Prof. Sonjoy Majumder, Dept. of Physics, IIT Kharagpur, whose constant guidance has been invaluable. Lekshmi Resmi acknowledges the Matrics grant MTR/2021/000830 of the Science and Engineering Research Board (SERB) of India. Debanjan Bose acknowledges the support of Ramanujan Fellowship-SB/S2/RJN-038/2017.

References

[1] Ray W Klebesadel, Ian B Strong, and Roy A Olson. Observations of gamma-ray bursts of cosmic origin. *The Astrophysical Journal*, 182:L85, 1973.

[2] Samuel B. Larson and Ian S. McLean. Extragalactic Content of Gamma-Ray Burst Localizations. , 491(1):93–113, December 1997.

[3] Pawan Kumar and Bing Zhang. The physics of gamma-ray bursts & relativistic jets. *Physics Reports*, 561:1–109, 2015.

[4] Yi-Zhong Fan, Tsvi Piran, Ramesh Narayan, and Da-Ming Wei. High-energy afterglow emission from gamma-ray bursts. *Monthly Notices of the Royal Astronomical Society*, 384(4):1483–1501, 02 2008.

[5] H. Abdalla, R. Adam, F. Aharonian, F. Ait Benkhali, E. O. Angüner, et al. A very-high-energy component deep in the γ-ray burst afterglow. *Nature*, 575(7783):464–467, November 2019.

[6] Peter Veres, PN Bhat, MS Briggs, WH Cleveland, R Hamburg, CM Hui, B Mailyan, RD Preece, OJ Roberts, A von Kienlin, et al. Observation of inverse compton emission from a long γ-ray burst. *Nature*, 575(7783):459–463, 2019.

[7] N Fraija, R Barniol Duran, S Dichiara, and P Beniamini. Synchrotron self-compton as a likely mechanism of photons beyond the synchrotron limit in grb 190114c. *The Astrophysical Journal*, 883(2):162, 2019.

[8] P. Kumar and R. Barniol Duran. On the generation of high-energy photons detected by the Fermi Satellite from gamma-ray bursts. , 400(1):L75–L79, November 2009.

PoS(ICRC2023)600

[9] F. Frontera et al. Spectral properties of the prompt x-ray emission and afterglow from the gamma-ray burst of 28 February 1997. *Astrophys. J. Lett.*, 493:L67, 1998.

[10] Tanima Mondal, Suman Pramanick, Lekshmi Resmi, and Debanjan Bose. Probing gamma-ray burst afterglows with the cherenkov telescope array. *Monthly Notices of the Royal Astronomical Society*, 522(4):5690–5700, 2023.

[11] Re'em Sari and Ann A. Esin. On the synchrotron self-compton emission from relativistic shocks and its implications for gamma-ray burst afterglows. *The Astrophysical Journal*, 548(2):787–799, Feb 2001.

[12] Abraham Achterberg, Yves A Gallant, John G Kirk, and Axel W Guthmann. Particle acceleration by ultrarelativistic shocks: theory and simulations. *Monthly Notices of the Royal Astronomical Society*, 328(2):393–408, 2001.

[13] R. Barniol Duran and P. Kumar. Implications of electron acceleration for high-energy radiation from gamma-ray bursts. *Monthly Notices of the Royal Astronomical Society*, 412(1):522–528, 03 2011.

[14] Bing Zhang. *The Physics of Gamma-Ray Bursts*. 2018.

[15] Taylor E. Jacovich, Paz Beniamini, and Alexander J. Van Der Horst. Modelling synchrotron self-Compton and Klein–Nishina effects in gamma-ray burst afterglows. *Mon. Not. Roy. Astron. Soc.*, 504(1):528–542, 2021.

[16] Ehud Nakar, Shin'ichiro Ando, et al. Klein–nishina effects on optically thin synchrotron and synchrotron self-compton spectrum. *The Astrophysical Journal*, 703(1):675, 2009.

[17] M Ackermann and M Ajello. o. allafort, a., the imprint of the extragalactic background light in the gamma-ray spectra of blazars. *Science*, 338.

[18] F. W. Stecker, O. C. de Jager, and M. H. Salamon. Tev gamma rays from 3c 279: A possible probe of origin and intergalactic infrared radiation fields. *ApJL*, 390(49), 1992.

[19] Alberto Dominguez, Joel R Primack, DJ Rosario, F Prada, RC Gilmore, SM Faber, DC Koo, RS Somerville, MA Pérez-Torres, P Pérez-González, et al. Extragalactic background light inferred from aegis galaxy-sed-type fractions. *Monthly Notices of the Royal Astronomical Society*, 410(4):2556–2578, 2011.

[20] E Massaro, Andrea Tramacere, M Perri, P Giommi, and G Tosti. Log-parabolic spectra and particle acceleration in blazars-iii. ssc emission in the tev band from mkn 501. *Astronomy & Astrophysics*, 448(3):861–871, 2006.

PoS(ICRC2023)600